Spectrally-Sliced Coherent Receiver Utilizing a Gain-Switched Optical Frequency Comb

Hilmi Othman, *Student Member, IEEE*, Xing Ouyang, *Member, IEEE*, Cleitus Antony, *Member, IEEE*, Frank Smyth, and Paul D. Townsend, *Member, IEEE*

***Abstract*—The spectrally-sliced coherent receiver is an attractive solution for future optical access network applications where cost is a sensitive factor, as it enables reduced bandwidth of the analog front-end components and analog-to-digital convertors when compared to a conventional intradyne coherent receiver. In a proof-of-concept experiment, we demonstrate a single-polarization 50 Gb/s QPSK C-band transmission experiment over 40 km of standard (G.652) fiber using receiver bandwidths as low as 6.25 GHz and also utilize an array of local oscillator lines derived from an injection locked gain-switched optical frequency comb, which can be realized as a compact photonic integrated circuit. This paper also analyses the influence of optical frequency comb properties on the quality of the reconstructed signal. The critical parameters considered in this study include comb power and flatness, mutual comb line coherence, and the comb line suppression ratio after demultiplexing the comb lines. We have shown that with practically achievable comb parameter values, the receiver can operate with less than a 1 dB sensitivity penalty compared to a conventional intradyne receiver. The scheme has the potential to provide a low-cost coherent receiver solution for next-generation access networks.**

***Index Terms*—Coherent detection, gain switching, optical fiber communication, optical frequency comb, optical receivers.**

I. Introduction

THE optical frequency comb (OFC) has proven to be a key component in a wide range of applications including mm-Wave and THz signal generation [1], [2], [3], [4], spectroscopy [5], [6], analog radio-over-fiber systems [7] and spectrally-efficient and flexible optical transceivers [8], [9]. In general, these applications exploit the high mutual coherence and fixed frequency spacing of the comb lines to achieve system benefits that are not attainable with multiple independent lasers.

Manuscript received 9 September 2022; revised 10 November 2022 and 18 January 2023; accepted 25 February 2023. Date of publication 13 March 2023; date of current version 16 August 2023. This work was supported in part by the Science Foundation Ireland under Grant 12/RC/2276_P2 and in part by the European Union's Horizon2020 under Grant 881158. *(Corresponding author: Hilmi Othman.)*

Hilmi Othman, Xing Ouyang, Cleitus Antony, and Paul D. Townsend are with the Photonics Systems Group, Tyndall National Institute, T12 R5CP Cork, Ireland, and also with the University College Cork, T12 K8AF Cork, Ireland (e-mail: hilmi.othman@tyndall.ie; xing.ouyang@tyndall.ie; cleitus.antony@tyndall.ie; paul.townsend@tyndall.ie).

Frank Smyth is with the Pilot Photonics, Invent Centre, Dublin City University, D09 PH2K Dublin, Ireland (e-mail: frank.smyth@pilotphotonics.com).

Color versions of one or more figures in this article are available at https://doi.org/10.1109/JLT.2023.3256180.

Digital Object Identifier 10.1109/JLT.2023.3256180

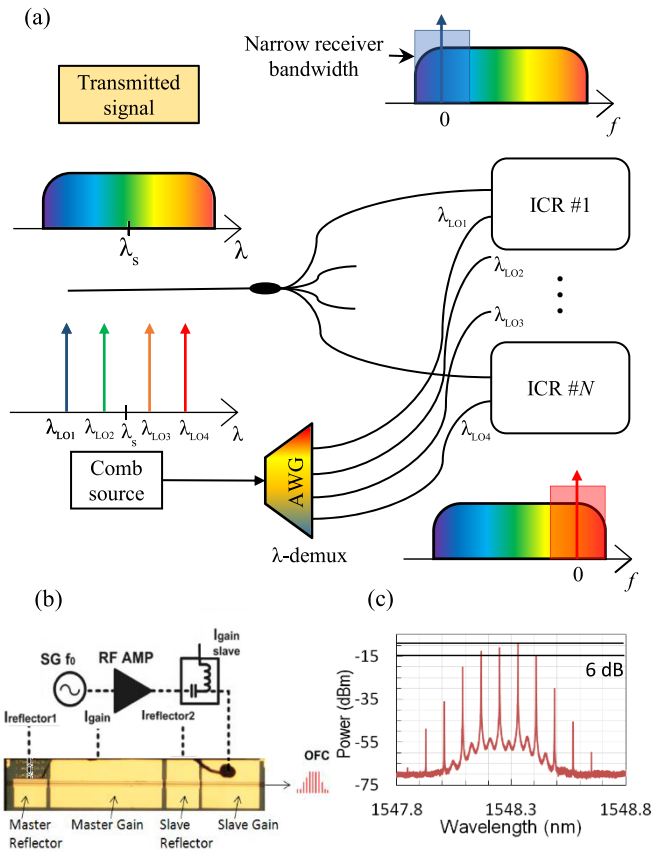

Fig. 1. (a) Schematic diagram of a spectrally-sliced optical coherent receiver enabled by an optical frequency comb. (a) The transmitted signal is split by a factor of *N* via an optical splitter and fed into an array of integrated *N*-coherent receiver (ICR) modules. The comb lines are separated by an optical demultiplexer and act as local oscillators that beat with the signal in each ICR to generate *N*-complex baseband signal slices following sub-signal bandwidth balance photodetection and ADC readout inside the ICRs. The signal reconstruction procedures are discussed on later sections. (b) Schematic of comb generation by injection locked gain-switched laser. Example of a manufactured PIC comprising two integrated lasers [27]. (c) Resultant gain switched OFC with four comb lines with 6 dB spectral ripple (flatness).

In addition to transmitter applications, the high mutual coherence of OFC sources can also be exploited in novel spectrally-sliced coherent receiver (SSRx) schemes. The SSRx is the optical analog of the well-known electronic frequency interleaved sampler [10], [11], [12]. As illustrated in Fig. 1(a), the SSRx contains an OFC that generates *N* coherent local oscillator (LO) lines, which enable the decomposition of a wideband signal

into N slices, each of which is detected by a separate conventional, but lower bandwidth, coherent receiver channel. This is followed by digital signal processing (DSP) to reconstruct the input waveforms in the digital domain [13], [14]. The SSRx has been studied in several contexts in optical communications including THz-scaling of data rate transmission up 1.2 Tb/s, enhanced reconstruction algorithm utilizing higher-order multi-input, multi-output structures [15], and Gardner timing error detector as a symbol synchronization method [16]. However, to the best of our knowledge, the SSRx has received comparatively less attention as a potential solution for coherent system applications in future passive optical networks (PON). Coherent PON has been the subject of much research attention in recent years [17] and cost reduction is one of the key concerns [18]. If we look at techno-economic trends in high speed PON, as exemplified by the latest ITU-T 50G PON standard [19], a general guiding principle is to exploit earlier generations of optical component technology which helps lower system cost, as volume markets which benefit from supply chain competition and amortization of production facility cost have already been established. Then, through the judicious use of DSP, to compensate for impairments that arise from performance deficiencies in these components. For example, the 50G standard envisages the use of 25G-class optoelectronics and employs digital equalizers to compensate for bandwidth limitations that would otherwise occur in a 50G NRZ modulation context. Due to the difficulty of meeting the large ($\sim$30 dB) power budget of point-to-multipoint PONs, the 50G standard may be the last to use conventional direct detection and NRZ modulation, which raises the question of whether coherent, with its higher receiver sensitivity and ability to fully compensate the effects of chromatic dispersion in the digital domain, may be required for future 100G or 400G PONs and beyond. Our motivation in this work is to explore whether spectral slicing could enable a continuation of the PON cost-reduction approach of exploiting older generations of component technologies, but now in the context of coherent PONs. The only cost-effective way to implement coherent transceivers is using photonic integrated circuits (PICs), so we frame our work within this context. The central principle is to exploit spectral slicing to reduce the bandwidth of the PIC receiver optoelectronics and with ideally only a modest increase in DSP complexity, and overall power consumption, enable signal recovery. In such a scenario, the RF bandwidths of the receiver photodiodes (PD), trans-impedance amplifiers (TIA), and analog-to-digital converters (ADCs), as well as the sampling rates of the ADCs, can be reduced by a factor of N, potentially enabling the use of high volume, low-cost and low power commodity components. In particular, high sampling rate ADCs contribute greatly to the cost and power consumption of a receiver [13]. If future anticipated advances in low-cost photonic integration can be harnessed to enable the required parallelisation of the optical components, then this reduction in the performance of the receiver RF front ends and ADCs may potentially be exploited to reduce the cost of coherent technology to open new applications in future PON.

There are several different techniques to generate OFCs, including mode-locked lasers (MLL) [20], [21], [22]; exploitation of the Kerr-nonlinearity in micro-ring resonators [22], [23], electro-optic modulator-based comb sources (EO OFC) [24], [25], [26], and gain-switched comb lasers (GS OFC) [27], [28]. Each of the techniques has its advantages and disadvantages depending on the application. For the spectrally-sliced receiver application that we motivate here, a key requirement is that the comb source is amenable to on-chip photonic integration to facilitate low-cost, compact transceiver fabrication. In addition, the OFC should ideally deliver sufficient power per comb line for the receiver to work in the shot-noise limited regime for optimum sensitivity [29]. Finally, for coherent communication, a comb source that offers low linewidth on each comb line is required. It is also important to consider the demultiplexer that separates the comb lines into the parallel receiver channels, which should have minimal footprint and complexity. Applying these general considerations to 100 Gbit/s QPSK systems, which may be the first coherent systems to be deployed in access networks [30], [31], suggests that a relatively modest number of comb lines, for example $N = 4$, with comb spacing of order 10 GHz (depending on signal spectral width) could provide a good compromise solution. This would enable the use of "10G class" components such as photodetectors, TIAs and ADCs, and, as we will show, require OFC and demultiplexer parameters that are practical and achievable. Commercially-available silicon PIC-based transceivers for the IEEE 400GBASE-DR4 standard and 4WDM Multi Source Agreement, employ 4×100G or 4×25G wavelengths to realise aggregate 400G or 100G data rates, respectively, which suggests that sufficiently high PIC yields can be achieved with parallelization on this scale.

Given these considerations, the paper will focus on the gain-switched laser-based OFC, as illustrated in Fig. 1(b)–(c). GS OFCs offer a number of advantages in terms of their potential for photonic integration, the ability to readily achieve the required comb spacing and to easily tune this spacing in response to signal bandwidth by varying the RF drive frequency. Other techniques have advantages in terms of generating very large numbers of comb lines, however that is not needed for this spectrally-sliced receiver application. Instead, the requirement is for a small number of comb lines with maximum power per line, which matches well with the GS OFC attributes. Alternative techniques such as Kerr micro-combs are currently less mature and more challenging to integrate given the two material systems required, and generally aim to generate much larger number of lines than required for this application. Similarly, MLLs are more challenging to integrate due to the typically used cleaved cavity and generate large numbers of lines as well. Moreover, MLLs typically have linewidths that are too large for this type of SSRx application [2].

Gain-switching with injection locking (IL-GS OFC) is a process to generate a high coherence train of optical pulses with repetition rates corresponding to the RF modulation frequency [32]. Such schemes have been proven in WDM transmission experiments achieving up-to 2 Tb/s on 24 channels [33], in radio-over-fiber systems [34], and the integration of IL-GS OFCs on an Indium Phosphide (InP) platform has also been demonstrated [28]. In this paper, the applicability of IL-GS OFCs to the spectrally-sliced receiver application through experiments and modelling are explored. In particular, this comb generation

technique is utilized to demonstrate single-polarization (SP) 25 GBaud QPSK (50 Gb/s) signal transmission over 40 km of single-mode fiber (SMF) using two SSRx channels ($N = 2$). Furthermore, the proposed scheme exhibits less than a 1 dB link penalty performance trade-off compared to a conventional (intradyne detection) receiver utilizing a 30 kHz linewidth external cavity laser (ECL) based LO.

The rest of this paper is organized as follows: Section II provides the system description and mathematical derivations of the proposed sliced signal reconstruction and Section III presents simulation results of SSRx performance as the key OFC characteristics are varied. Then, the experiment setup and results are discussed in Sections IV and V respectively. Finally, conclusions are drawn in Section VI.

II. Spectrally-Sliced Concept

The transmitted data a_m, for a single channel transmission can be represented in the form of a baseband signal as:

$$\mathrm{s}(t) = \sum_m a_m \, \mathrm{h_{Tx}} \left(\mathrm{t} - mT_s \right), \tag{1}$$

considering that the pulse shape $h_{\mathrm{Tx}}(t)$ (representing the overall transmitter system response) is applied to the signal which has a symbol period T_s. The data is then applied to an I/Q modulator to modulate a laser beam with a centre frequency of f_c. The transmitted single-carrier optical signal with phase noise term of φ_s can then be written as

$$E_s(t) \; = \; s(t) \, e^{j \; 2\pi \; f_c \; t \; + \; \varphi_s} \; . \tag{2}$$

The optical fiber channel can introduce signal impairments arising from chromatic and polarization mode dispersion, fiber nonlinearities, and amplified spontaneous emission from optical amplifiers. However, only the ideal case of a back-to-back system is considered, in order to focus on the numerical theory of the SSRx detection and reconstruction processes. For this application, a frequency comb with N comb lines with frequencies that lie within the signal bandwidth and are centred on f_c is required. Therefore, the optical field for the frequency comb can be expressed as

$$\sum_{n \; = \; 1}^{N} \sqrt{P_{\mathrm{LO},n}} e^{j 2\pi \; (f_{\mathrm{LO},n} \; t \; + \; \varphi_{\mathrm{LO}})},$$

where

$$f_{\mathrm{LO},n} = (n \; - \; 1) \; f_{\mathrm{FSR}} + f_{\mathrm{LO}} \; , \tag{3}$$

and $P_{\mathrm{LO},n}$ represents the optical power of the n-th line, φ_{LO} is the phase term for the comb line assuming that the comb has perfect phase locking, and f_{FSR} and f_{LO} represent the free spectral range frequency and the frequency of the first mode of the comb respectively. As shown in Fig. 1(a), in the SSRx, the transmitted signal is split into N identical copies, and the frequency comb lines are demultiplexed and utilized as LOs. These LOs beat with the whole signal spectrum in N parallel coherent receiver branches to convert the optical signal into N sampled slices. The representation of the signal field from (2), and the optical comb tone E_{LO} for the n-th coherent receiver input can be re-written as:

$$E_{\mathrm{sig},n}(t) = \sqrt{\frac{P_s \, (t)}{N}} \; e^{\, j2\pi (f_c \; t \; + \; \varphi_s(t))},$$

$$E_{\mathrm{LO},n}(t) = \sqrt{P_{\mathrm{LO},n}} \; e^{\, j2\pi (f_{\mathrm{LO},n} \; t \; + \; \varphi_{\mathrm{LO}}(t))}, \tag{4}$$

where P_s denotes the signal power. Assuming that each split signal and LO are co-polarized, and using coherent detection, the complex output photocurrent comprising in-phase (I) and quadrature components (Q) generated from the n-th coherent receiver can be reconstructed as:

$$I_c(t) = \; 2R \sqrt{\frac{P_s \, (t)}{N} \; P_{\mathrm{LO},n}} \; e^{\, j2\pi (\Delta f_n \; t \; + \; \varphi_s(t) \; + \; \varphi_{\mathrm{LO}}(t))}, \tag{5}$$

where R is the PD responsivity, and the offset frequency between the carrier and n-th LO comb line is given by $\Delta f_n = f_c - f_{\mathrm{LO},n}$. Each photocurrent is then fed into an ADC, modelled as the combined baseband impulse response of the overall receiver (balanced photodetector and ADC), $\mathrm{H_{Rx},}_n$ with the assumption that any skew between the I and Q channels has been calibrated and compensated for. Given that the N OFC lines are within the signal spectral bandwidth and are equally spaced, $\mathrm{H_{Rx},}_n$ can be optimized with slice bandwidth, $\mathrm{BW_{Slice}}$ as

$$\mathrm{BW_{Slice}} = \; B/2N, \tag{6}$$

where B denotes the transmitted signal bandwidth. In order to build a signal reconstruction chain, some assumptions concerning the frequencies and bandwidths of the signal, OFC, and slices are made as follows:

- All slice bandwidths are identical to each other ($H_{\mathrm{Rx},n}$) and lie within the signal spectrum bandwidth.
- If N is odd, the $[(N + 1) / 2]$ -th tone is centred at f_c, having only small offset, and constant over transmitted symbols.
- If N is even, both $N/2$ and $[(N / 2) + 1]$ -th lines are equally spaced from f_c, having only small offset, and constant over transmitted symbols.

Based on the aforementioned assumptions, the sampled received signal at the output of each n-th coherent receiver can be represented as

$$u_n(t) = \left[\sum_{t \; = \; -1/2T_s}^{1/2T_s} s(t \;) \; h_{\mathrm{Tx}}(t) \; h_{\mathrm{Rx},n}(t) \right] \times \; e^{\, j2\pi (\Delta f_n \; T_s \; t \; + \; \varphi_s(t) \; + \; \varphi_{LO}(t))}, \tag{7}$$

then, the overall output signal, $\hat{U}_n(f)$ can be reconstructed by merging all the signal slice tributaries in the digital domain. This can be achieved by numerically shifting each of the signal slice frequencies by Δf_n in the time domain before a linear superposition of all these mixing products is performed. Each frequency-shifted slice can be written in the frequency domain as

$$\hat{U}_n(f \; - \; \Delta f_n) = \; \mathcal{F}^{-1} \left\{ u_n(t) \cdot (j \; 2\pi \; \Delta f_n) \right\}, \tag{8}$$

where the $\mathcal{F}^{-1}\{\cdot\}$ term is the inverse Fourier transform operation. Assuming amplitude and phase matching on all slices, then the recovered 'stitched' signal can be written as follows:

$$\hat{U}_n(f \;) = \sum_{n \; = \; 1}^{N} \hat{U}_n(f \; - \; \Delta f_n), \tag{9}$$

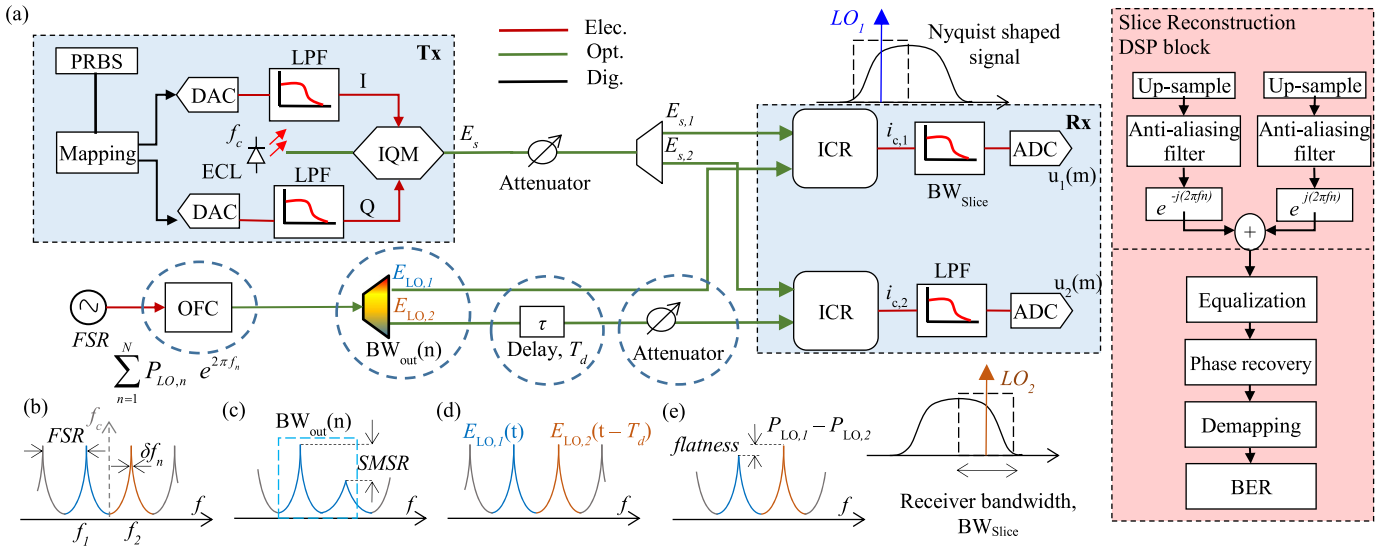

Fig. 2. (a) Simulation system model of transmitter and receiver (blue blocks) for a spectrally-sliced coherent system using $N = 2$ slices. LPF: low-pass filter, FSR: free-spectral range, BW: bandwidth,ICR: integrated coherent receiver, inset (Red block): Block diagram of signal reconstruction DSP. Schematic comb spectra at various points in the experiment illustrating key parameters for consideration. (b) Comb linewidth and free spectral range (FSR). (c) Comb line side-mode suppression ratio after demultiplexing. (d) Phase coherence of comb line. (e) Comb amplitude flatness.

Using the above conceptual principles, the parallel coherent detection approach can be realized as long as N-comb lines are utilized in the bandwidth of signal spectrum. Therefore, increasing the number of slices N results in a reduction of the bandwidth requirement for each receiver branch by a factor of N. However, the splitting of the signal also introduces a factor of N power loss - hence the SNR of the signal degrades. The stitching process can be performed in DSP where the complexity for this operation scales linearly with N. Based on the modest value of N we motivate in this paper, the number of additional steps is minimal and adds only minimally to the overall DSP complexity, which is dominated by the conventional coherent signal recovery steps [35]. In deriving (8), we assumed the ideal case of coherent amplitude and phase matching of all signal slices, which requires an ideal OFC source generating equal amplitude tones with perfect phase locking and negligible relative phase noise. However, with practical OFCs, $P_{\mathrm{LO},n}$ and $\varphi_{\mathrm{LO},n}$ may differ for each slice tributary, hence in the next section, the main focus is on how the SSRx system performance is affected by these non-ideal practical factors.

III. Simulations

In this section, the performance of the proposed spectrally-sliced receiver is compared with a conventional coherent receiver ($N = 1$) and it is shown how the OFC's properties affect the quality of the reconstructed signal in a transmission link. VPI-TransmissionMaker was used to simulate the optical transmitter and SSRx setup as shown in Fig. 2, while MATLAB was used to perform the DSP to generate and recover the baseband signal. The simplest case of $N = 2$ spectral slices was analysed for consistency with the later experiments, however the conclusions are valid for larger numbers of slices. At the transmitter, pseudo-random bit sequences (PRBS) of length $2^{15} - 1$ were first generated and shaped to a 25 GBaud, quadrature phase-shift keying (QPSK) Nyquist signal with a 10% roll-off factor raised-cosine filter. Hence, the model simulates one of the polarization channels in a 100 Gb/s polarization-multiplexed QPSK system. The transmitter-launched power was set at 0 dBm and an optical attenuator was included in the transmission link to vary the optical power detected by the receiver. Based on (6), the receiver bandwidths were designed with Bessel functions of 12.5 GHz and 6.25 GHz, for the conventional and SSRx cases respectively. The applied filtering is used to emulate all of the bandwidth limitations arising from the photo-receiver electronics. Cascaded phase and intensity modulators were used to generate the LO frequency comb lines from a single laser to emulate the ideal, highly correlated case. Unless otherwise stated, the power per LO comb line was set to +10 dBm, for consistency with the later experiments. Following detection, the signal was sampled at 50 GSa/s and 25 GSa/s, for the conventional and SSRx schemes respectively, before being sent to the DSP for signal reconstruction and recovery. The DSP blocks that perform these functions are shown in Fig. 2, with only the lower half of the processing chain used for the conventional receiver case. The DSP includes an adaptive equalization (AEQ) step using a 7-tap equalizer based on the constant-modulus algorithm with tap-weights initialized by a training-aided least-mean-squared equalizer, and carrier phase compensation (CPE) using Viterbi-Viterbi phase estimation. As for 16-state quadrature amplitude modulation (16-QAM) modulation format; the QPSK partitioning algorithm was used [36]. Finally, after demapping, the signal quality was calculated based on the bit-error rate (BER) counting. The rest of the simulation parameters are listed in Table I.

To establish a baseline of ideal SSRx system performance, the analysis of BER versus received signal power was simulated for a range of (per line) LO comb powers, as shown in Fig. 3(a). The results follow the same trend obtained for the conventional

TABLE I
SIMULATION PARAMETERS

Device Parameter		Laser Parameter	
LO power, $P_{LO,n}$	+10 dBm (unless otherwise specified)	Central wavelength, λ_c	1559.0 nm
PD responsivity, R	0.7 A/W	Linewidth, δf	100 kHz
Tx pulse shaping roll-off	0.1	Comb Spacing, f_{FSR}	12.5 GHz
Thermal noise	10 pA/$\sqrt{\text{Hz}}$	**General Parameter**	
Slice bandwidth, BW_{Slice}	6.25 GHz	Symbol Rate, B_d	25 GBaud
Conventional bandwidth, $BW_{Conventional}$	12.5 GHz	Num. of Pol	1
ADC resolution	8 bits	Pattern Length	PRBS 15

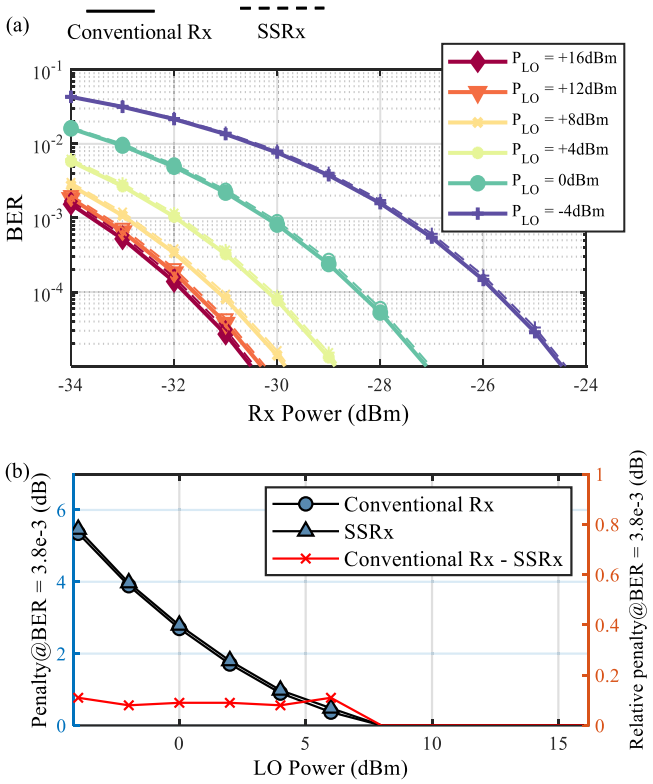

Fig. 3. (a) BER versus received signal power for different local oscillator power, P_{LO} and two different detection schemes: conventional coherent receiver (solid line) and ($N = 2$) spectrally-sliced coherent receiver (dashed lines) respectively for 25 GBaud QPSK signals. (b) Simulated receiver sensitivity penalty as a function of local oscillator power.

intradyne receiver, with the highest sensitivity achieved in the shot noise-limited, high LO power region, and a progressive degradation of sensitivity, due to dominating receiver thermal noise, as the LO power decreases. Fig. 3(b) shows the power penalty for the SSRx versus the conventional receiver, evaluated at a BER of 3.8×10^{-3} relative to +16 dBm LO power of each scheme. It can be seen that there is almost negligible performance penalty between the two receiver schemes across the full LO power range. Fig. 4(a) and (b) show the reconstruction DSP procedures to stitch two signal slices together. Note that, for

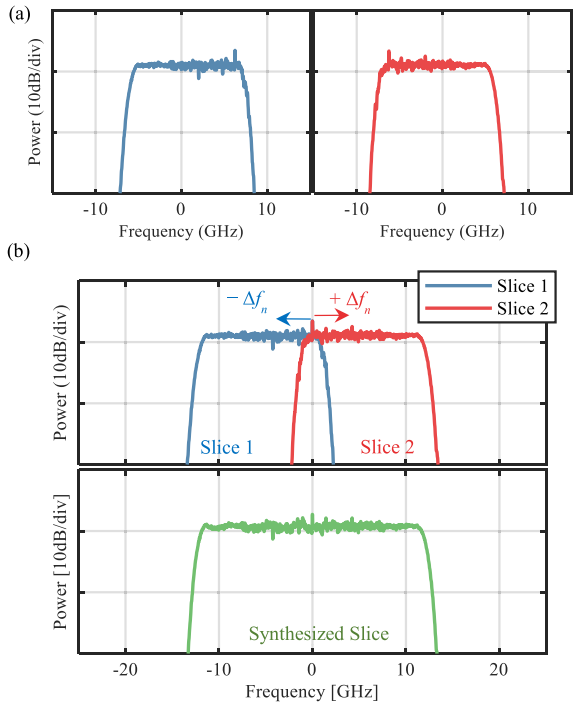

Fig. 4. Simulated spectra illustrating the digital signal reconstruction procedures. (a) Digital spectral slices for receiver 1 (left) and receiver 2 (right) respectively. (b) Top: Digitized frequency-shifted spectral slices. Bottom: Reconstructed spectrum of a 25 GBaud QPSK signal.

approximately equal performance, the SSRx requires the same power per LO comb line after demultiplexing as the single LO in the conventional receiver. If the total LO power in the SSRx is constrained to be the same as for the conventional receiver case, then the degree of performance degradation can be estimated from Fig. 3(a) for the $N = 2$ case. For example, to compare against a conventional receiver with an LO power of +10 dBm, an $N = 2$ comb source of equal total power would generate +7 dBm per comb line. Assuming a 3 dB demultiplexer loss gives +4 dBm per comb line, which translates to a performance power penalty less than 1.0 dB at a BER of 3.8×10^{-3}. However, it is possible to reduce the impact on system performance, by employing an active demultiplexer co-integrated with the comb source. This approach has been demonstrated in a PIC platform [43] and shown to simultaneously increase both comb line power and comb-line suppression ratio, which, as we show in Section III-C, improves spectrally-sliced system performance.

Having established the baseline performance of the SSRx, we now proceed to simulate how some of the key parameters that characterize a practical OFC source affect this performance.

A. Spectral Flatness

The amplitude difference between the OFC comb lines termed as spectral flatness, is one of the key parameters affecting OFC performance in an optical communication system [7]. In the spectrally-sliced receiver application, spectral flatness and channel to channel insertion loss variations in the associated demultiplexer lead to variations in local oscillator power, P_{LO} across the N slices. After signal mixing and detection, this

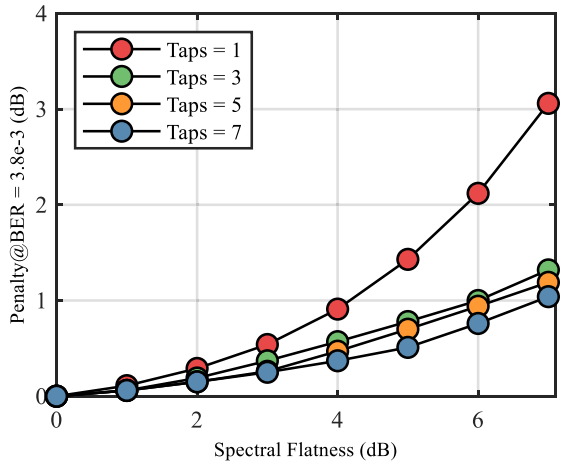

Fig. 5. Simulated sensitivity penalty versus the spectral flatness generated by comb source relative to spectral flatness of 0 dB.

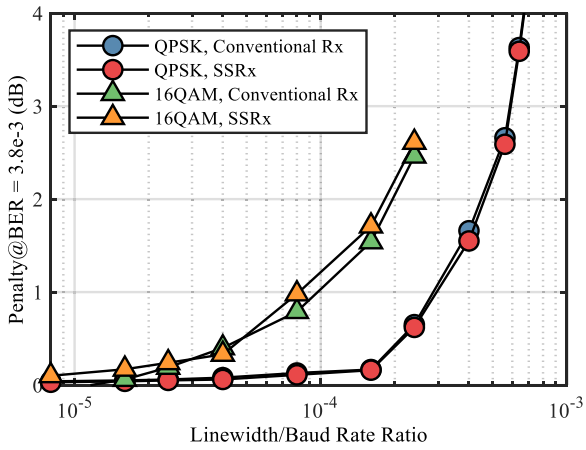

Fig. 6. Simulated sensitivity penalty as a function of product of the laser linewidth δf and symbol duration $1/B_d$ for two different modulation formats. QPSK: Quadrature phase-shift keying, 16-QAM: 16-state quadrature amplitude modulation.

variation leads to amplitude imbalances between slices that can degrade the quality of the reconstructed signal. This effect was emulated in the simulations for the $N = 2$ case by attenuating the optical power of one comb line with respect to the other. Specifically, one of the LO powers was varied from $+3$ to $+10$ dBm, while the other was fixed at $+10$ dBm, giving a spectral flatness ranging from 7 to 0 dB.

The sensitivity penalty was measured with respect to the SSRx's performance for different values of the number of taps in the adaptive equalization step following reconstruction operation with 0 dB spectral flatness ($P_{LO,1} = P_{LO,2} = +10$ dBm). As shown in Fig. 5, the SSRx system performance degrades as the spectral flatness parameter increases. This is an easily understood consequence of the increased contribution of thermal noise in the low LO power receiver branch, which degrades the total SNR of the reconstructed signal. In addition, as the amplitude mismatch between the two slices increases, a larger number of equalizer taps are required to compensate for the mismatch to achieve optimum reconstruction performance. As PIC-based combs can readily achieve spectral flatness values of less than 3 dB, we expect that, with the optimized equalization taps, the impact of this factor can be of the order of 0.3 dB or less in terms of sensitivity penalty.

B. Phase Noise

The optical linewidth of the local oscillator laser is one of the most crucial factors for coherent system performance in optical fiber communications, especially when higher-order modulation formats are employed [37]. For the comb source, the seed laser that generates the optical carrier for the RF signal applied to the modulator will have phase noise that is quantified by the laser linewidth, δf as an easy-to-handle figure of merit. The linewidth represents the spectral width of a lorentzian spectral line associated with a white frequency independent FM noise spectrum [38]. The phase noise of the comb is contained within the term φ_{LO} from (5) and can be expressed as

$$\varphi_{\mathrm{LO}}\ (t) = \varphi\,(t-1) + \Delta\varphi\,(t) \tag{10}$$

where $\Delta\varphi$ is the zero-mean gaussian random variable with variance defined by $2\pi\delta f/B_d$ where B_d is the symbol rate. This distortion can be estimated and compensated using the M-th power feedforward DSP scheme [39].

The impact of linewidth and symbol duration product ($\delta f/B_d$) on the performance of the SSRx and the conventional coherent receiver were simulated for two different modulation formats, QPSK and 16-QAM. To ensure that the phase noise from the OFC (as LO) was dominant in the system, the transmitter laser was modelled as an ideal source with zero linewidth. The phase estimation was performed using certain number of symbol block averaging, and the sensitivity penalty was calculated with respect to the transmission performance without the LO phase noise ($\delta f = 0$). The results are shown in Fig. 6. The same tolerance trends for both receiver schemes were observed, and as expected, 16-QAM is less tolerant to phase noise than QPSK, since more discrete phases need to be discriminated for correct symbol detection. For a 1 dB penalty, the maximum tolerable linewidth and symbol duration product is around 3.0×10^{-4} and 0.8×10^{-4} for QPSK and 16-QAM, respectively, for both receiver schemes. This result shows that the SSRx has the same phase noise tolerance as a conventional coherent receiver. As will be shown in Section V, the IL-GS OFC used in the experiments has a linewidth of approximately 300 kHz giving a linewidth and symbol duration product of 1.2×10^{-5} at 25 GBaud. Hence, the results shown in Fig. 6 confirm the feasibility of using this OFC in the SSRx to achieve low phase noise penalties.

C. Side Mode Suppression Ratio (SMSR)

A key element of the SSRx is the OFC demultiplexer which is used to select the LO tone for each sliced receiver channel. Practical demultiplexers, have non-zero inter-channel crosstalk, which in the SSRx application results in some leakage of adjacent LO tones into a given receiver channel. This leads to additional beat products in the reconstructed signal that may impair the performance of the SSRx. The simulations to investigate the impact of this affect were performed for varying levels

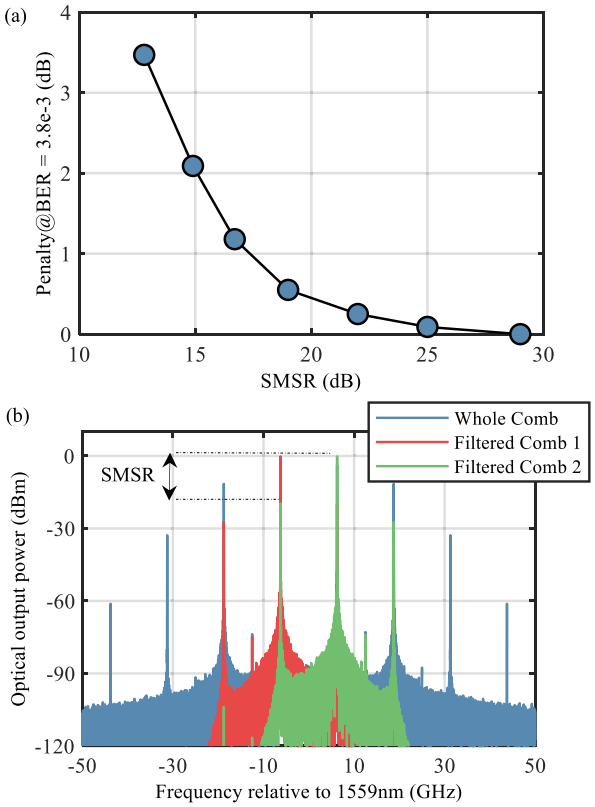

Fig. 7. (a) Simulated sensitivity penalty versus SMSR for the SSRx detection. (b) Spectra captured for the whole frequency comb (blue), and two isolated combs filtered by demultiplexer with finite bandwidth (red and green).

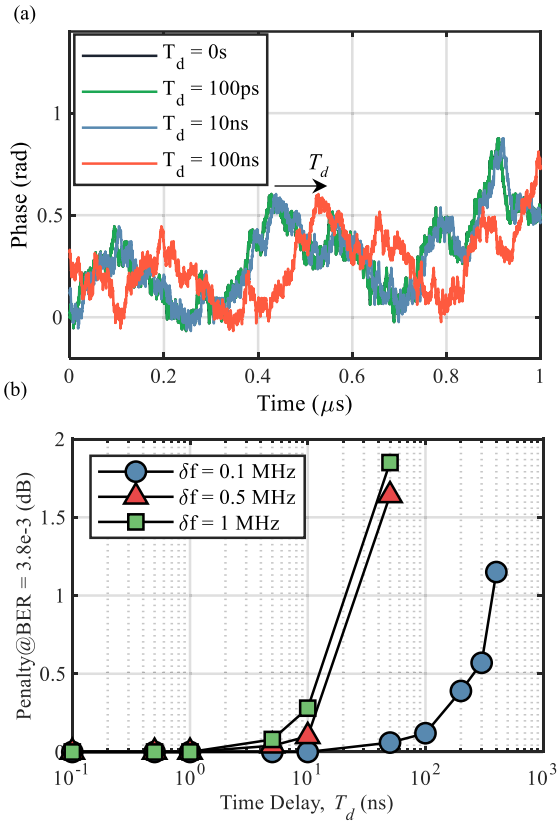

Fig. 8. (a) Phase noise traces of comb line ($\delta f = 100$ kHz) with delayed versions of itself. (b) Simulated sensitivity penalty versus the applied time delay for three different linewidth.

of SMSR, calculated as $P_{LO} - P_{SM}$ (dB), where the first term corresponds to the power of the desired tone and the latter term is the power of the dominant side tone. To vary the SMSR in the simulations the filter bandwidth of the comb demultiplexer was varied. The spectrum of the filtered comb lines is shown in Fig. 7(b). As the bandwidth of the filter broadens, the adjacent tone's power increases, hence reducing the SMSR. Fig. 7(a) shows the simulated sensitivity penalty as a function of the SMSR for the SSRx scheme. It can be observed that for a higher SMSR (>20 dB), the sensitivity penalties induced are below 0.5 dB, which highlights the importance of the SMSR for high quality signal reconstruction performance of the SSRx system. Note that, research on InP-based active comb demultiplexer has shown that SMSR values of this magnitude are attainable in OFC PICs [40].

D. Mutual Coherence

Finally, the impact of one of the OFC's key properties, namely the degree of phase correlation between the comb lines was investigated. In practical OFCs, phase correlation is affected by the fundamentals of the comb generation process in the OFC laser cavity as well as by the injection locking process when an external, narrow-linewidth master laser is used, as in the IL-GS OFC case. In addition, where external RF modulation is employed, noise from the driver electronics, could, in principle, also generate decorrelation. Our numerical model uses a single master laser followed by external electro-optic modulators to create the OFC, and hence simulates the ideal case of perfect correlation. However, the decorrelation was emulated by adding a relative time delay, T_d to one of the comb line paths following demultiplexing. This is carried out by circularly shifting the numerical array representing the optical field of the LO comb line by the number of sample points corresponding to T_d. Hence, the phase difference of the two comb lines can be written as

$$\varphi_{\mathrm{LO},1}(t) - \varphi_{\mathrm{LO},2}(t - T_d). \tag{11}$$

Fig. 8(a) shows an example of a simulated phase trajectory for one of the LO lines, and the impact of the applied time-shift for various values of T_d. When T_d is zero, both LO lines will have identical phase trajectories. However, as T_d increases an instantaneous phase decorrelation between the two LO lines is generated. The impact of this decorrelation on the SSRx system performance is presented in Fig. 8(b) for various values of linewidth, δf. It can be seen that, as long as the time delay is small compared to the inverse linewidth, the performance penalty is negligible. For the 300 kHz linewidth IL-GS OFC used in the experiments, this translates to a relative time delay of around 12 ns for less than 1 dB sensitivity penalty, which is easily satisfied in a PIC implementation. However, as discussed above, practical OFC's suffer from other sources of phase decorrelation, even when the receiver channel path lengths are well-matched, so this was an important factor to study in the following experiments.

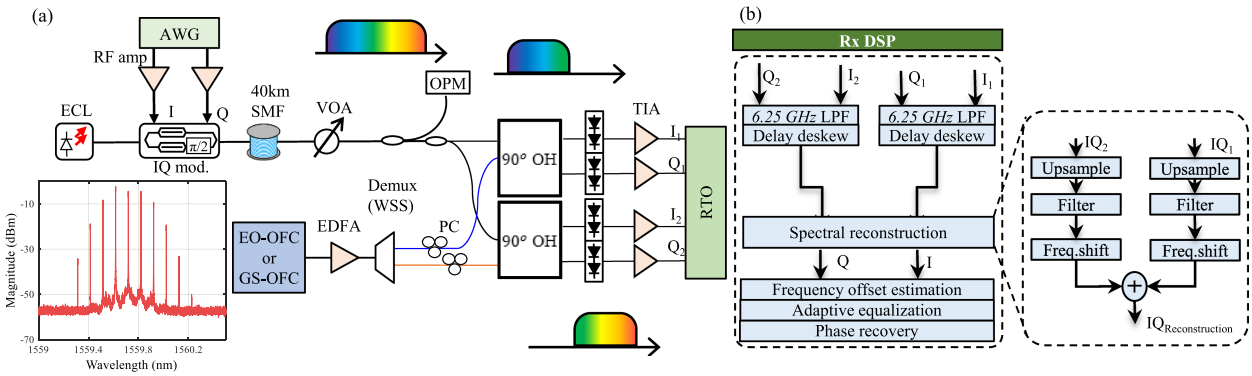

Fig. 9. (a) Experimental setup for 50 Gb/s SP-QPSK with ($N = 2$) SSRx over 40 km of SMF, VOA: variable optical attenuator, OPM: optical power meter, OH: optical hybrid, TIA: transimpedance amplifier, WSS: wavelength selective switch. Inset: the optical spectrum of the injection locked gain-switched optical frequency comb with 0.16 pm resolution. (b) The DSP blocks used for recovering sliced signals. Note that, 6.25 GHz low pass filters are implemented digitally on both complex slices to emulate the bandwidth reduction advantage of the spectrally-sliced approach.

IV. Experimental Setup

To demonstrate the feasibility of the proposed SSRx detection scheme ($N = 2$) with an IL-GS OFC, we perform a proof-of-concept experiment using the testbed illustrated in Fig. 9(a). The transmitted signal was generated by a tunable ECL with a 30 kHz linewidth and a wavelength of 1559.53 nm which was modulated with 25 GBaud QPSK signals generated by an IQ Lithium Niobate (LN) Mach-Zehnder modulator (MZM) driven by two PRBS ($2^{15} - 1$) signals from the 50 GSa/s arbitrary waveform generators (AWG). Note that, a root-raised cosine filter (0.1 roll-off) was applied to both I/Q components before DAC conversion, resulting in a complex signal bandwidth of 25 GHz. The optical signal from the transmitter (launch power = +4 dBm) propagates across a 40 km span of optical fiber (Corning SMF28E+) before the signal is attenuated by an optical attenuator which is used to vary the received power. At the receiving end, the SSRx was constructed from two integrated SP coherent receivers with front-end bandwidths of 25 GHz, which employ neighboring comb lines (separated by a wavelength selective switch (WSS) and amplified to +10 dBm each) as LOs. The polarization controller (PC) ensures that the LOs and the signal are co-polarized to each other. Finally, the I and Q signals from the two receivers were sampled by two-synchronized real-time oscilloscopes (RTO) operating at 100 GSa/s (bandwidth = 33 GHz) before the sampled waveforms are stored for offline signal processing. The DSP to recover and measure the system performance by BER counting was performed in MATLAB. Fig. 9(b) shows the processing steps used in this experiment. Firstly, the two parallel complex inputs, corresponding to the slice 1 and slice 2 signals, were filtered in the digital domain with a 6.25 GHz low-pass filter to prove the potential for bandwidth reduction. This was followed by a deskewing operation to compensate for the path delay introduced by cable length mismatches. In the signal reconstruction step, both complex slices were resampled and then frequency-translated to the original slice centre frequencies (±6.25 GHz) before the slices were then stitched together. Following reconstruction, further standard coherent signal recovery processing steps were taken. First, the phase and amplitude mismatches between overlapping regions of the slices were equalized adaptively with optimized complex-valued weight through the radius-directed algorithm after performing coarse frequency offset compensation (CFO). This was followed by feedforward phase recovery based on the Viterbi-Viterbi algorithm to compensate the phase noise before evaluation of the signal quality.

To estimate the performance of the SSRx scheme, we analyze the quality of the reconstructed 25 GBaud QPSK signals obtained with LOs generated by the EO OFC and the IL-GS OFC respectively, and compare these with the performance using a conventional SP intradyne coherent receiver (LO, $\delta f = 30$ kHz). In this proof-of-concept experiment, due to limited equipment availability, only two comb lines ($N = 2$) and SP operation were used, but in principle, the concept can be readily scaled to dual polarization operation and larger numbers of slices subject to the maximum number of lines generated by the OFC. Given our transmitted complex signal spectral width is approximately 25 GHz; the required comb line spacing is 12.5 GHz, which generates two slices with minimum bandwidth. The GS semiconductor laser-based OFC (Pilot Photonics Lyra-1000) was used to generate five main comb lines with spacing of 12.5 GHz as shown in Fig. 9(a).

In order to characterize the FM-noise spectrum of the IL-GS OFC used for this experiment, we used a similar comb experiment and method to that discussed in [41], which is based on analysis of the phase-noise of beat signals simultaneously recovered from a digital coherent receiver [42]. For this OFC characterization work, another tunable ECL of 30 kHz linewidth was used as a reference to mix with each comb line in a coherent receiver. The corresponding waveforms were then captured by the RTO before offline processing of the sampled complex signals performed using MATLAB. Note that, the waveforms were captured at 50 GSa/s and each record was of length of 20 μs. The same procedures were also applied to characterize the phase noise of the EO OFC for comparison.

Finally, the impact of SMSR variations on SSRx performance was analyzed. In these and the other reported experiments, the WSS passband was set to its minimum width of approximately 10 GHz. This is similar to the 12.5 GHz frequency spacing of the OFCs used in the experiments, and hence, is the main

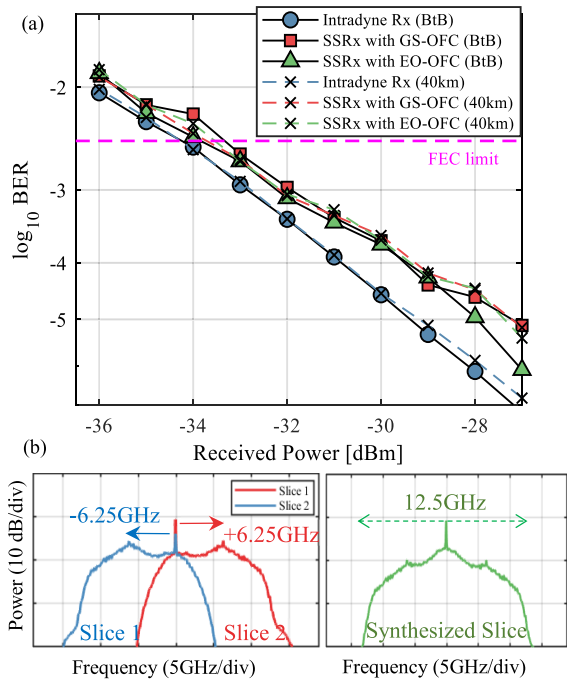

Fig. 10. (a) Receiver power sensitivity performance of the conventional and proposed SSRx for 25 GBaud QPSK signals. Results obtained by comparing conventional Rx with the proposed SSRx utilizing IL-GS OFC and EO OFC. For SSRx-based reception, there is less than 1 dB sensitivity penalty observed on both OFC variants even though the bandwidth for each receiver branch is halved. (b) Digitized and frequency-shifted by ±6.25 GHz spectral slices (red, blue) and synthesized 25 GBaud data signal (green) spectra.

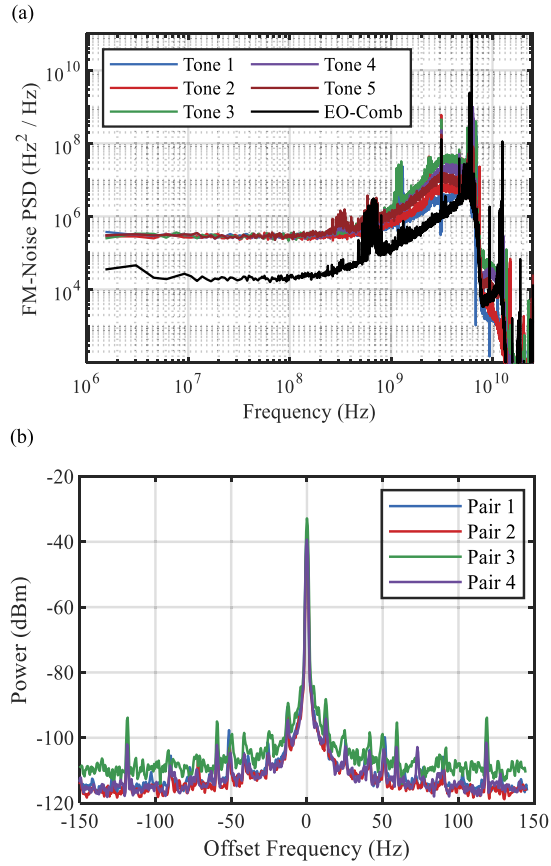

Fig. 11. (a) Calculated FM-noise spectrums for both EO OFC tones and for IL-GS OFC (all five main tones). (b) RF beat tones generated between the pair of comb lines for all four IL-GS OFC pairs captured at 12.5 GHz offset frequency (RBW = 3 Hz, VBW = 3Hz).

factor limiting the achievable SMSR values. In order to study the impact of SMSR over a wider range of values than was achievable with the IL-GS OFC, the EO OFC was also used and the SMSR was varied by adjusting the RF amplitude driving the modulator.

V. Experimental Results and Discussions

In this section, we present and discuss the main experimental results obtained during the study. Firstly, the BER performance versus received optical power for both detection schemes; conventional intradyne coherent receiver and SSRx utilizing both OFC variants are shown in Fig. 10(a) for the back-to-back (BtB) and 40 km SMF transmission cases. For a fair comparison, the output power per comb line in the SSRx scheme is matched with the LO output power in the conventional receiver case. The BER performance is very similar in all cases, although the SSRx cases show small 0.5 dB (EO OFC) and 0.9 dB (IL-GS OFC) sensitivity penalties at FEC limit of 3.8×10^{-3} (HD FEC with 7% overhead), compared to the conventional receiver. Note that, this similar performance is achieved with receiver bandwidths that are reduced by half (to 6.25 GHz) in the SSRx case, compared with the conventional receiver. The small additional 0.4 dB penalty in the IL-GS OFC case, compared to the EO OFC scheme was investigated and is due to lower SMSR of each demultiplexed comb line. The results for 40 km fiber and BtB transmission are very similar, indicating that the sliced signal reconstruction does not significantly affect the performance of the dispersion equalizers. As 20 km reach is the standard for access network today, 40 km represents a reasonable benchmark covering potential future reach extensions. The spectra in Fig. 10(b) illustrates the signal reconstruction process, showing the digitized frequency-shifted sliced signals corresponding to the spacing of comb lines (left), and the reconstructed spectrum after the stitching process (right).

As mentioned earlier, the FM-noise spectra of both OFCs were measured to enable an evaluation and comparison of the phase noise. The intermediate frequencies (IF) of the sampled complex waveforms were estimated, shifted to the origin, then a 5 GHz low-pass filter was applied digitally to remove excess noise from the unwanted adjacent tones. Next, the optical phase was obtained by unwrapping the phase of the waveform trajectories. Then, differentiation was performed to retrieve the instantaneous frequency fluctuations as a function of time. Hence, the frequency dependent FM-noise spectral density profiles, $S_{FM}(f)$, can be retrieved, and the optical linewidth can be estimated from the white FM-noise components. As shown in Fig. 11(a), the IL-GS OFC exhibits similar FM-noise spectra for each of the five main tones, with a corresponding measured linewidth of ∼300 kHz. For the EO OFC case, the observed linewidth for the two filtered comb lines is around ∼30 kHz, thus presenting a negligible deviation from the source laser (ECL). This is

expected given the relatively low additional noise introduced by the RF source, driver, and modulators in the electro optic comb generation process. It might be thought that, the higher linewidth of the IL-GS OFC is responsible for the slightly higher penalty measured in the transmission experiments. However, as shown by the previous simulation results in Fig. 6, negligible penalty is expected for 25 GBaud QPSK modulation and a 300 kHz comb linewidth. To check other possible explanations, a further investigation was made to assess the phase correlation properties of the IL-GS OFC across the four comb line pairs. For each pair, the two consecutive comb lines, with separation frequency of 12.5 GHz, were filtered and heterodyned on a 12.5 GHz photo receiver. The beat signal was then captured by an electrical spectrum analyzer (ESA) with a narrow resolution bandwidth (RBW = 3 Hz). Fig. 11(b) shows the consistent and very narrow full width at half-maximum of the beating tones which is around a few Hz, indicating a high degree of phase correlation between all comb line pairs. This result indicates that the relative phase coherence times between comb line pairs are of the order of tenths of seconds, which we note is very much longer than the 20 μs record lengths used for data acquisition in our experiments. Hence, we do not expect any significant performance impairments due to this factor.

To gain further insight into the effectiveness of signal reconstruction with varying SMSR, the SSRx sensitivity with different pairs of the IL-GS OFC's comb lines were evaluated. For a fair comparison, in each case the LO power per comb line was fixed at the same power using EDFAs and VOAs in the experiment. However, since the IL-GS OFC has non-zero comb flatness, this leads to an SMSR after demultiplexing that varies from line to line. The results are shown in Fig. 12(a). The measured SSRx sensitivity varies from −33 to −31 dBm across the four sets of comb pairs as shown by the red points. The SMSR values for each of the comb tones are also shown, and it can be seen that when the SMSR of one or both of the tones is low, the receiver sensitivity is correspondingly low. To further quantify and explain this effect, the sensitivities of the SSRx were evaluated using the EO OFC with different values of SMSR obtained by adjusting the modulator drive conditions. The EO OFC was used for this experiment as higher maximum SMSR values could be obtained compared to the IL-GS OFC, which enabled a sweep from the zero to large sensitivity penalty limits to be made. As shown by the results in Fig. 12(b), for a penalty of less than 0.5 dB, the allowable SMSR for both demultiplexed lines should be 20 dB or higher, in good agreement with the modelling results shown in Fig. 7(a). This explains the variation in SSRx sensitivity measured with different IL-GS OFC comb line pairs shown in Fig. 12(a). In particular, the 2nd and 3rd comb line pairs degrade the SSRx sensitivity by around 2 dB compared to the best sensitivity case obtained for the 1st comb line pair. The IL-GS OFC SSRx performance data in Fig. 10(a) was obtained using this best-case pair, for which the minimum SMSR was approximately 21 dB (tone B). In comparison, the EO OFC SMSR was 25 dB for this experiment. Hence, the additional 0.4 dB penalty observed for the IL-GS OFC based SSRx can be explained as being due to the poorer SMSR compared to the EO OFC. This SMSR was limited by the minimum filter width of

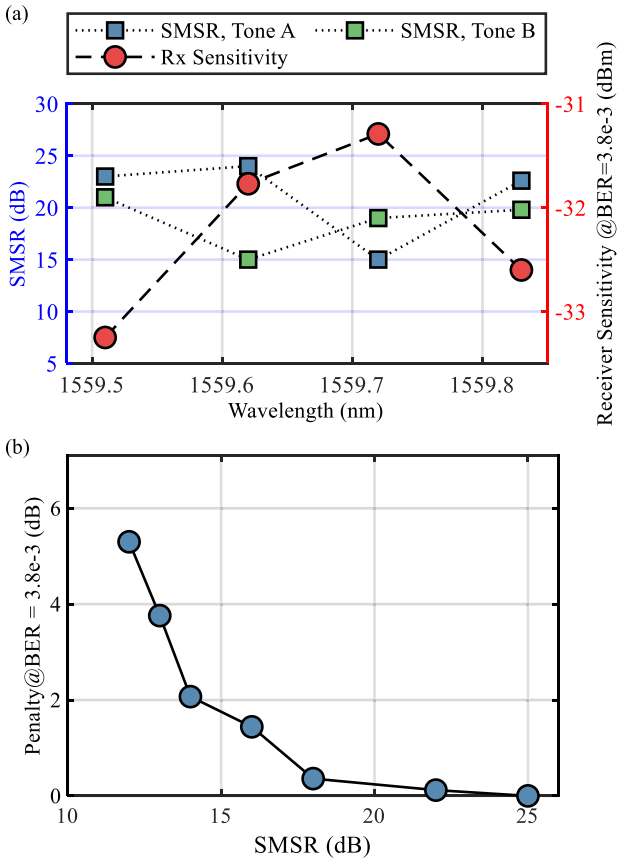

Fig. 12. (a) Measured receiver sensitivity performance of the SSRx obtained with the IL-GS OFC. Trace red (right y-axis) represents the measured receive sensitivity of the SSRx for four sets of comb pairs, while the SMSR measured for the demultiplexed comb tones in each pair is represented by the blue and green (left y-axis) traces. (b) Measured sensitivity penalty versus SMSR of the SSRx obtained with the EO OFC.

the WSS used in the experiments and can be readily improved by using alternative demultiplexers, such as active solutions, which not only improve the side-tone rejection ratio, but also provide amplification, noise reduction, and gain flattening [43].

It is also important to compare the spectral slicing approach with other potential future coherent PON solutions that also offer opportunities for receiver bandwidth reduction. Digital subcarrier multiplexing (DSCM) technology as proposed in [44] is one such candidate. In [44], the authors take the example of a 64 GBaud single wavelength carrier signal and show how it can be replaced by 16 non-overlapping subcarriers (SC) at 4 GBaud with DSCM. In a point-to-multipoint PON scenario, all or a subset of these SC can be selected at a given PON terminal by a coherent receiver with appropriate bandwidth. In the extreme case, if only one sixteenth of the total data rate is required at the terminal, then a single SC can be selected and the receiver bandwidth can be reduced by a factor of sixteen compared to the single carrier case, However, equally this is then the maximum data rate available at the terminal and any increase requires an equipment upgrade by either increasing the single receiver bandwidth, or by increasing the number of narrow bandwidth receivers, proportionate to the number of SC desired for detection.

TABLE II
POLARIZATION AND PHASE DIVERSITY COHERENT RECEIVERS

	Intradyne	DSCM [45]	SSRx
Baud Rate	64 GBaud	16 × 4 GBaud	64 GBaud
Transmitter	1×ECL + 2×IQ Mod	1×narrow linewidth ECL + 2×IQ Mod + DSC Mux DSP	1×ECL + 2×IQ Mod
Rx Analog BW / Number of Component	4×Class 40 (BPD + TIA + ADC)	For *M*=1, 4×Class 40 (BPD + TIA + ADC) @ For *M*=2, 8×Class 20 (BPD + TIA + ADC)	For *N* = 2, 8×Class 20 (BPD + TIA + ADC)
Rx DSP	MIMO + CFO + CPE	DSC Demux + low-speed parallel DSP	Reconstruction + MIMO + CFO + CPE
Downstream / Upstream	TDM /TDMA	DSCM / TFDM	TDM / TDMA
Bandwidth Provision	Flexible	Granularity of subcarrier	Flexible

Due to the larger symbol period in DSCM, narrower linewidth lasers are required compared to the single channel case, and in the case of upstream communications the uncorrelated phase noise from different transmitters will accumulate. In contrast, in spectral slicing, we employ conventional time division multiplexing / multiple access (TDM/TDMA) with a single carrier transmitter and a highly correlated comb source at the receiver which preserves laser linewidth tolerance, since in the upstream and downstream cases only one transmitter laser is transmitting at any given instant in time. In addition, the TDM/TDMA protocol allows fine granularity bandwidth sharing and statistical multiplexing, which is important for mixed service provision and efficient, dynamic use of bandwidth. The latter would be challenging for DSCM as low symbol rates and narrow SCs translate to the need for very high laser stability. The spectral slicing approach enables the bandwidth of the receiver front end to be reduced by a factor of N, which as mentioned may be particularly advantageous for simplifying burst-mode receiver design in the upstream channel case. In summary, the two approaches have different merits which we summarize from the coherent receiver aspect in Table II (using the system specification in [44]), also comparing with the conventional single channel receiver case. In the case of spectral slicing, the full signal bandwidth is received and reconstructed from N slices, so, for fairness, we compare the equivalent performance case for DSCM where all SC are detected by M coherent receivers, with bandwidth $1/M$ times the full signal bandwidth. Assuming upstream laser phase noise accumulation is not too detrimental, then DSCM also enables reduced receiver front-end bandwidth, however spectral slicing offers the additional advantage of maintaining the TDM/TDMA feature of current PONs, which enables fine granularity bandwidth provisioning without incurring additional laser linewidth constraints.

VI. CONCLUSION AND OUTLOOKS

In this paper, we have reported and investigated the results of numerical simulations and experimental tests of an SSRx utilizing an array of local oscillator lines derived from an optical frequency comb. Specifically, we have focused on an OFC based on an injection locked gain-switched semiconductor laser, which can be realized as a compact PIC, and we have elucidated the key OFC attributes required for successful signal reconstruction. The study highlighted the impact of the comb source's phase noise and phase correlations in determining the quality of signal reconstruction as well as impairments due to the parasitic beat tones, which can arise from imperfect spectral flatness and adjacent comb line rejection. In particular, we have motivated the use of such a scheme to reduce the bandwidths of the analog front-end components and ADCs when compared to conventional intradyne coherent receivers and speculated on the potential exploitation of this advantage in future coherent access networks. The potential for bandwidth reduction was demonstrated experimentally via a single-polarization 50 Gb/s QPSK C-band transmission experiment over 40 km of standard (G.652) fiber using receiver bandwidths as low as 6.25 GHz, with $N = 2$ slices. The reduction of receiver front-end bandwidth is particularly useful in the context of a PON upstream burst-mode receiver, which must operate at high dynamic range ($\sim$20 dB) and quickly adapt its gain within a few hundred nanoseconds at the start of each burst on a burst-by-burst basis. This component becomes increasingly difficult to realize as bandwidth and linearity requirements increase, making the spectral slicing approach particularly valuable in this context. With access to larger numbers of receiver channels, which could be facilitated by photonic integration, the scheme can readily be extended to dual polarization 100 Gb/s operation, and beyond. For example, a 200 Gb/s dual polarization 50 GBaud QPSK system with $N = 4$ slices could be realized with an IL-GS OFC similar to the one used in this work and with the same receiver bandwidth. Burst-mode receivers of this bandwidth already exist and are widely commercially deployed, albeit not yet developed for coherent detection. If the IL-GS OFC linewidth can be reduced further, then in principle higher order modulation format such as 16-QAM and beyond can be supported. To the best of our knowledge, our work represents the first SSRx demonstration using a highly integratable comb source such as IL-GS OFC. In future work, we plan to explore the use of PIC-based IL-GS OFC with integrated active demultiplexers to demonstrate a route toward the goal of a fully integrated, low cost spectrally sliced receiver.

ACKNOWLEDGMENT

The authors would like to acknowledge Dr. Giuseppe Talli for many helpful discussions and suggestions in the early stages of this work.

REFERENCES

[1] M. Imran, P. M. Anandarajah, A. Kaszubowska-Anandarajah, N. Sambo, and L. Potí, "A survey of optical carrier generation techniques for Terabit capacity elastic optical networks," *IEEE Commun. Surv. Tut.*, vol. 20, no. 1, pp. 211–263, Firstquarter 2018.

[2] H. Hu and L. K. Oxenløwe, "Chip-based optical frequency combs for high-capacity optical communications," *Nanophotonics*, vol. 10, no. 5, pp. 1367–1385, Feb. 2021.
[3] C. Browning, D. Dass, P. Townsend, and X. Ouyang, "Orthogonal chirp-division multiplexing for future converged optical/millimeter-wave radio access networks," *IEEE Access*, vol. 10, pp. 3571–3579, 2022.
[4] L. Lundberg et al., "Phase-coherent lightwave communications with frequency combs," *Nature Commun.*, vol. 11, no. 1, Jan. 2020, Art. no. 201.
[5] I. Coddington et al., "Dual-comb spectroscopy," *Optica*, vol. 3, no. 4, Apr. 2016, Art. no. 414.
[6] C. Quevedo-Galán et al., "Gain-switched semiconductor lasers with pulsed excitation and optical injection for dual-comb spectroscopy," *Opt. Exp.*, vol. 28, no. 22, Oct. 2020, Art. no. 33307.
[7] C. Browning et al., "Gain-switched optical frequency combs for future mobile radio-over-fiber millimeter-wave systems," *J. Lightw. Technol.*, vol. 36, no. 19, pp. 4602–4610, Oct. 2018.
[8] J. Lin, H. Sepehrian, Y. Xu, L. A. Rusch, and W. Shi, "Frequency comb generation using a CMOS compatible SiP DD-MZM for flexible networks," *IEEE Photon. Technol. Lett.*, vol. 30, no. 17, pp. 1495–1498, Sep. 2018.
[9] M. Mazur et al., "High spectral efficiency coherent superchannel transmission with soliton microcombs," *J. Lightw. Technol.*, vol. 39, no. 13, pp. 4367–4373, Jul. 2021.
[10] N. K. Fontaine et al., "Fiber nonlinearity compensation by digital backpropagation of an entire 1.2-Tb/s superchannel using a full-field spectrally-sliced receiver," in *Proc. 39th Eur. Conf. Exhib. Opt. Commun.*, 2013, pp. 1–3.
[11] N. K. Fontaine et al., "Real-time full-field arbitrary optical waveform measurement," *Nature Photon.*, vol. 4, no. 4, pp. 248–254, Apr. 2010.
[12] C. Zhang, Y. Mori, K. Igarashi, K. Katoh, and K. Kikuchi, "Ultrafast digital coherent receiver based on parallel processing of decomposed frequency subbands," in *Proc. 36th Eur. Conf. Exhib. Opt. Commun.*, 2010, pp. 1–3.
[13] J. C. M. Diniz et al., "Digital signal processing for spectrally-sliced coherent optical receivers," in *Proc. Eur. Conf. Opt. Commun.*, 2015, pp. 1–3.
[14] G. Gao and L. Lei, "Photonics-based broadband RF spectrum measurement with sliced coherent detection and spectrum stiching technique," *IEEE Photon. J.*, vol. 9, no. 5, Oct. 2017, Art. no. 5503111.
[15] V. E. S. Parayba et al., "Digital nonlinear compensation for spectrally sliced optical receivers with MIMO reconstruction," *IEEE Photon. Technol. Lett.*, vol. 28, no. 22, pp. 2589–2592, Nov. 2016.
[16] V. N. Rozental, A. L. N. Souza, S. M. Rossi, A. Chiuchiarelli, J. R. F. D. Oliveira, and J. D. Reis, "Time recovery for spectrally-sliced optical receivers," in *Proc. 42nd Eur. Conf. Opt. Commun.*, 2016, pp. 1–3.
[17] D. Lavery et al., "Opportunities for optical access network transceivers beyond OOK [Invited]," *J. Opt. Commun. Netw.*, vol. 11, no. 2, pp. A186–A195, Feb. 2019.
[18] V. Houtsma, A. Mahadevan, N. Kaneda, and D. van Veen, "Transceiver technologies for passive optical networks: Past, present, and future [Invited Tutorial]," *J. Opt. Commun. Netw.*, vol. 13, no. 1, pp. A44–A55, Jan. 2021.
[19] "Higher speed passive optical networks: Requirement," ITUT-Recommendation G.9804.1, 2019. [Online]. Available: https://www.itu.int/rec/T-REC-G.9804.1-201911-I/en
[20] K. Zeb et al., "InAs/InP quantum dash buried heterostructure mode-locked laser for high capacity fiber-wireless integrated 5G new radio fronthaul systems," *Opt. Exp.*, vol. 29, no. 11, May 2021, Art. no. 16164.
[21] J. Hauck et al., "Semiconductor laser mode locking stabilization with optical feedback from a silicon PIC," *J. Lightw. Technol.*, vol. 37, no. 14, pp. 3483–3494, Jul. 2019.
[22] L. Chang et al., "Integrated optical frequency comb technologies," *Nature Photon.*, vol. 16, no. 2, pp. 95–108, Feb. 2022.
[23] J. Pfeifle et al., "Full C and L-Band transmission at 20 Tbit/s using cavity-soliton Kerr frequency combs," in *Proc. Conf. Lasers Electro-Opt.*, 2015, Paper JTh5C-8.
[24] M. Imran et al., "12.5GHz-100GHz tunable spacing optical carrier source for flexgrid bandwidth variable transponders," in *Proc. Int. Conf. Opt. Netw. Des. Model.*, 2015, pp. 157–161.
[25] S. Liu et al., "Optical frequency comb and Nyquist pulse generation with integrated silicon modulators," *IEEE J. Sel. Topics Quantum Electron.*, vol. 26, no. 2, Mar./Apr. 2020, Art. no. 8300208.
[26] Y. Hu et al., "High-efficiency and broadband on-chip electro-optic frequency comb generators," *Nature Photon.*, vol. 16, no. 10, pp. 679–685, Aug. 2022.
[27] M. D. G. Pascual, V. Vujicic, J. Braddell, F. Smyth, P. Anandarajah, and L. Barry, "Photonic integrated gain switched optical frequency comb for spectrally efficient optical transmission systems," *IEEE Photon. J.*, vol. 9, no. 3, Jun. 2017, Art. no. 7202008.
[28] M. D. G. Pascual et al., "InP photonic integrated externally injected gain switched optical frequency comb," *Opt. Lett.*, vol. 42, no. 3, pp. 555–558, Feb. 2017.
[29] K. Kikuchi and S. Tsukamoto, "Evaluation of sensitivity of the digital coherent receiver," *J. Lightw. Technol.*, vol. 26, no. 13, pp. 1817–1822, Jul. 2008.
[30] G. Rizzelli Martella, A. Nespola, S. Straullu, F. Forghieri, and R. Gaudino, "Scaling laws for unamplified coherent transmission in next-generation short-reach and access networks," *J. Lightw. Technol.*, vol. 39, no. 18, pp. 5805–5814, Sep. 2021.
[31] D. Nesset, "PON roadmap [Invited]," *J. Opt. Commun. Netw.*, vol. 9, no. 1, pp. A71–A76, Jan. 2017.
[32] P. M. Anandarajah et al., "Generation of coherent multicarrier signals by gain switching of discrete mode lasers," *IEEE Photon. J.*, vol. 3, no. 1, pp. 112–122, Feb. 2011.
[33] J. Pfeifle et al., "Flexible terabit/s Nyquist-WDM super-channels using a gain-switched comb source," *Opt. Exp.*, vol. 23, no. 2, pp. 724–738, 2015.
[34] H. Shams et al., "100 Gb/s multicarrier THz wireless transmission system with high frequency stability based on a gain-switched laser comb source," *IEEE Photon. J.*, vol. 7, no. 3, Jun. 2015, Art no. 7902011.
[35] B. S. G. Pillai et al., "End-to-end energy modeling and analysis of long-haul coherent transmission systems," *J. Lightw. Technol.*, vol. 32, no. 18, pp. 3093–3111, Sep. 2014.
[36] I. Fatadin, D. Ives, and S. J. Savory, "Laser linewidth tolerance for 16-QAM coherent optical systems using QPSK partitioning," *IEEE Photon. Technol. Lett.*, vol. 22, no. 9, pp. 631–633, May 2010.
[37] C. Yu et al., "Bit-error rate performance of coherent optical M-ary PSK/QAM using decision-aided maximum likelihood phase estimation," *Opt. Exp.*, vol. 18, no. 12, pp. 12088–12103, May 2010.
[38] M. G. Taylor, "Phase estimation methods for optical coherent detection using digital signal processing," *J. Lightw. Technol.*, vol. 27, no. 7, pp. 901–914, Apr. 2009.
[39] J. Cheng, C. Xie, M. Tang, and S. Fu, "Hardware efficient adaptive equalizer for coherent short-reach optical interconnects," *IEEE Photon. Technol. Lett.*, vol. 31, no. 15, pp. 1249–1252, Aug. 2019.
[40] M. D. Gutierrez et al., "Monolithically integrated 1x4 comb de-multiplexer based on injection locking," in *Proc. 18th Eur. Conf. Integr. Opt.*, 2016, pp. 18–20.
[41] K. Zanette et al., "Correlation properties of the phase noise between pairs of lines in a quantum-dot optical frequency comb source," in *Proc. Opt. Fiber Commun.Conf.*, 2017, pp. 1–3.
[42] K. Kikuchi, "Characterization of semiconductor-laser phase noise and estimation of bit-error rate performance with low-speed offline digital coherent receivers," *Opt. Exp.*, vol. 20, no. 5, pp. 5291–5302, Feb. 2012.
[43] A. Kaszubowska-Anandarajah et al., "Reconfigurable photonic integrated transmitter for metro-access networks," *J. Opt. Commun. Netw.*, vol. 15, no. 3, pp. A92–A102, Mar. 2023.
[44] D. Welch et al., "Point-to-multipoint optical networks using coherent digital subcarriers," *J. Lightw. Technol.*, vol. 39, no. 16, pp. 5232–5247, Aug. 2021.

Hilmi Othman (Student Member, IEEE) received the master's degree in electronics & communication engineering from The University of Sheffield, Sheffield, U.K., in 2014. He is currently working toward the Ph.D. with Tyndall National Institute, Cork, Ireland. From 2014 to 2019, he was a Photonics Researcher with Telekom Malaysia Research and Development, Malaysia, where he has been involved in several fiber-to-the-home research projects. Commencing in 2019, he is with the Photonic System Group under supervision of Prof. Paul Townsend. His current research focuses on use of coherent optics for optical access networks.

Xing Ouyang (Member, IEEE) received the Ph.D. degree from Tyndall National Institute, University College Cork, Cork, Ireland, in 2017. He is currently a Senior Researcher with Photonics System Group, Tyndall National Institute, University College Cork. His research interests include high-speed fiber-optic and wireless communications, microwave photonics and radio-over-fiber systems, digital signal processing, and integrated sensing and communications. Moreover, he is recognized as the inventor of orthogonal chirp-division multiplexing (OCDM), which is an emerging multicarrier modulation technology for future high-speed optical and wireless access systems and radar systems, and based on the technology he is leading a R&D team for a pre-commercialization initiative, ChirpComm.

Cleitus Antony (Member, IEEE) received the Ph.D. degree in physics from Tyndall National Institute, Cork, Ireland, in 2011, which contributed to record-breaking experimental demonstrations in advanced high-capacity fibre to the home networks. From 2001 to 2006, he was an Engineer with Hitachi's World-Class Fibre Optic Division, Opnext Japan Inc., Yokohama. He has 15 years of experience as a Researcher of optical communications and worked on several EU and national projects on research topics that span novel optical network architectures, optical amplification strategies, and digital signal processing techniques. He is currently a Staff Senior Researcher with the Photonics Systems Group, Tyndall. He holds five patents and has authored more than 50 peer-reviewed publications. His recent research interests include exploiting machine learning to advance next-generation optical communication systems and circuits.

Frank Smyth received the Ph.D. degree from Dublin City University, Dublin, Ireland, in 2009, having carried out pioneering research on novel tunable laser sources and optical switching systems. He is Co-Founder and CTO of Pilot Photonics Ltd, an Irish company developing unique optical comb lasers based on photonic integration. His previous position was Co-Founder and Executive Director of the CONNECT Centre for Future Networks for which he helped secure significant research funding from Science Foundation Ireland and from Industry. He held a Scholarship position with Bell Laboratories, Crawford Hill, NJ, USA, and a Research Fellowship with Dublin City University, Dublin, Ireland, before founding Pilot Photonics in 2011. He has raised VC investment and research funding to develop its unique technology including the prestigious European Innovation Council (EIC) Accelerator award. He has co-authored more than 95 research publications, contributed to six patent applications, and was an Expert Reviewer of photonics and optical communication for the *Journal of Lightwave Technology*, and European Commission. He is currently a Member of the Industry Advisory Board of the CONNECT Research Centre with Trinity College Dublin.

Paul D. Townsend (Member, IEEE) received the Ph.D. degree in physics from the University of Cambridge, Cambridge, U.K., in 1987. Between 1987 and 1990, he held Research Fellowship positions with St John's College, Cambridge, U.K. and Bell Communications Research (Bellcore), Red Bank, NJ, USA, where he worked on non-linear optical switching phenomena in polymeric semiconductors. In 1990, he joined British Telecom Laboratories, Martlesham Heath, U.K., as a Senior Staff Researcher to lead activities on Quantum Communications and Cryptography. In 2001, he joined the Corning Research Centre, Martlesham Heath, U.K., as the Head of Group for Access Network Research. Since 2003, he has been with the Tyndall National Institute, University College Cork (UCC), Cork, Ireland, where he is currently the Head of Photonics Research, Director of the Science Foundation Ireland IPIC National Photonics Research Centre, and a Professor of photonic systems research with the School of Physics, UCC. He is a Fellow of the Institute of Physics (U.K. and Ireland), and has authored or coauthored more than 250 publications, including 35 invited conference papers, and holds granted patents in 16 families. His research interests include photonic systems and enabling technologies for optical communications.